Design and Analysis of a Novel ZVZCT Boost Converter With Coupling Effect

Xi Zhang, *Senior Member, IEEE*, Wei Qian, and Zhe Li

***Abstract*—In this paper, a new zero voltage zero current transition (ZVZCT) boost DC–DC converter using a coupled inductor is proposed. This topology provides the main switch ZVZCT for the turn-on and zero voltage switching (ZVS) for the turn-off. Moreover, the auxiliary switch turns on at zero current switching (ZCS) and turns off at ZVS. The main diode turns on with ZVT and turns off with ZCS, and other diodes also operate under soft-switching conditions. Besides, due to the coupling effect, the proposed converter improves efficiency additionally since resonant energy in the resonance tank could be transferred to the output, and the circulating current can be limited as well. The soft-switching can be realized in almost all the load rang. In this design, there always exist energy releasing circuits to conduct magnetic flux leakage currents, such that the surge currents are eliminated and switch current stress can be accordingly reduced. All the devices resonate in a unique direction within less than half of a resonance period, so power losses with respect to the resonance can be decreased. In this paper, the converter design and operation principles of the converter are given. It also has been verified by a 1-kW experimental prototype with switching frequency of 100 kHz, and the related experimental results are presented.**

***Index Terms*—Auxiliary switch, boost DC–DC converter, coupling effect, zero voltage zero current transition (ZVZCT).**

I. Introduction

THE pulse width modulation (PWM) DC–DC converters are widely used due to their high power density, fast response, and control simplicity. Boost converters, as a kind of common converters, are utilized in various areas, such as the power source, battery charger, hybrid energy storage system, power factor correction (PFC), photovoltaic (PV) generation system, and so on [1]–[6]. In order to solve switching losses and electromagnetic interference with switching frequency increasing [7], deployment of the soft-switching technology is feasible [8].

In order to realize soft-switching, adopting additional resonant circuits is considered as a common approach [9]–[14]. In [12], the main switch is exposed to significant current stress. In [13] and [14], the main switch turns off at ZCT without increasing the current stress, and the auxiliary switch operates with SS, but its voltage stress of the main diode is twice the output voltage. Some studies (e.g., [15]) solve the problems above, however it is obvious that there are overlaps of current and voltage waveforms on the auxiliary switch, so the turn-off process is not perfect. In the system proposed in [16], the main switch ZVT turn-on and ZCT turn-off were implemented, however, for the auxiliary switch, only a "nearly" zero current switching (ZCS) turn-off is provided.

In some studies for interleaved soft-switching converters [17]–[25], compared to conventional boost converters, more components and more complicated control strategies are required. In [19], two conventional boost converters are connected in parallel, and an additional inductor that connects two phases is adopted to generate zero voltage switching (ZVS) conditions for two MOSFETs. In [21], the main switches can achieve ZVS and ZCS simultaneously. In [22], there are three interleaved phases, and the inductor current of each phase is bidirectional, which supplies the inverse current to conduct the body diode. The similar topology was presented in [23], where the inductors of two phases are coupled to reduce the total size. However, for interleaved structures, the control strategies are relatively complicated. In many coupled-inductor-related studies such as [26] and [27], the inductors are coupled totally, however once the coupling coefficient is not very close to one, power losses of parasitic oscillations and surge currents occur due to the leakage inductance.

In this study, a novel ZVZCT boost converter with coupling effect is proposed, which solves most of the aforementioned problems. In order to reduce the iron core loss, size, and cost of the converter, three inductors share the same iron core. Moreover, it is not necessary to have all inductors coupled totally. Since the new topology is capable of conducting the leakage inductance current through energy releasing loops, the parasitic oscillations and surge current can be eliminated as aforementioned. In the meantime, the auxiliary winding in the coupled inductor can help implement ZVS conditions. The coupled inductor transfers electromagnetic energy in the resonance tank to the output due to the coupling effect, reducing the current of the auxiliary switch, so its conduction loss is reduced and the efficiency is improved additionally. The new converter provides the main switch ZVZCT turn-on and ZVS turn-off. The auxiliary switch operates with ZCS turn-on and ZVS turn-off, respectively. The main diode turns on at ZVT and turn off at ZCS, and the rest of diodes are also under soft-switching conditions. All the devices resonate in a unique direction within less than half of resonance period, which can improve efficiency, as

Manuscript received November 7, 2016; accepted January 11, 2017. Date of publication January 19, 2017; date of current version August 2, 2017. This work was supported in part by the National Natural Science Foundation of China (NSFC) under Grant 51677118 and in part by the Science and Technology Commission of Shanghai Municipality (STCSM) under Grant 16PJD030. Recommended for publication by Associate Editor C. Fernandez.

The authors are with the School of Mechanical Engineering, Shanghai Jiao Tong University, Shanghai 200240, China (e-mail: braver1980@sjtu.edu.cn; weiwei_nuaa@163.com; 316248853@qq.com).

Color versions of one or more of the figures in this paper are available online at http://ieeexplore.ieee.org.

Digital Object Identifier 10.1109/TPEL.2017.2655584

well. Soft-switching maintains for almost all input voltage and load ranges.

The comparison between the existing topologies (e.g., [15]) and the proposed one in this study has been made as follows. In [15], the auxiliary switching frequency is twice the main switching frequency, so the main switching frequency could not be increased very high due to the frequency limitation of the auxiliary switches. Meanwhile, too many operating modes affect reliability and stability, and the volume and weight are also affected by using more inductors. In this study, the auxiliary switching frequency is independently decided, so the main switching frequency can reach high. In addition, less operating modes or inductors exist in this paper. In most converters similar to that in [15], the average current in the auxiliary switch is larger than the input current, which mainly contributes to ZVT for the main switch. Unfortunately, the limitation of the current stress will influence the ZVT realization. It results in the ZVT operation at a fragile boundary. Circuits will lose ZVT or even be destroyed by slight load change. In this study, the topology could easily limit the average current of the auxiliary switch by shrinking the peak current interval. Therefore, when the load changes, the proposed converter could maintain the SS conditions.

This topology not only focuses on achieving soft-switching under wide variable load, but also on avoiding serious resonant circulation. So it has obvious advantages in some applications, e.g., the electric vehicular system with a wide range of load changes due to complicated driving conditions. In addition, it is also suitable for the PV system and charging stations with large load changes. Good conversion efficiency could be achieved in the proposed topology, which is beneficial for the overall efficiency enhancement of the aforesaid systems. Normally the input and output voltage for the proper applications could be from tens to hundreds of volts, and the power rate could be from hundreds to thousands of watts. The switching frequency is limited by the interior characteristics of the switches.

The rest of the paper is organized as follows: the topology configuration and operation principles are described in Section II. Parameter analysis is provided in Section III. Experimental results are obtained and analyzed in Section IV and conclusions are given in Section V.

II. Topology Configuration and Operation Principles

As shown in Fig. 1(a), the resonance part consists of a coupled-inductor, two resonant capacitors, four diodes, and an auxiliary switch. Cr_1 includes the parallel capacitor and the parasitic capacitor of the main switch S_1. The decoupling expression of the voltage and current for the coupled inductors could be written as follows:

$$\begin{bmatrix} v_{L1} \\ v_{La1} \\ v_{Lb1} \end{bmatrix} = \begin{bmatrix} L_1 & M_{a1} & -M_{b1} \\ M_{a1} & L_{a1} & -M \\ -M_{b1} & -M & L_{b1} \end{bmatrix} \begin{bmatrix} \dfrac{di_{L1}}{dt} \\ \dfrac{di_{La1}}{dt} \\ \dfrac{di_{Lb1}}{dt} \end{bmatrix} \tag{1}$$

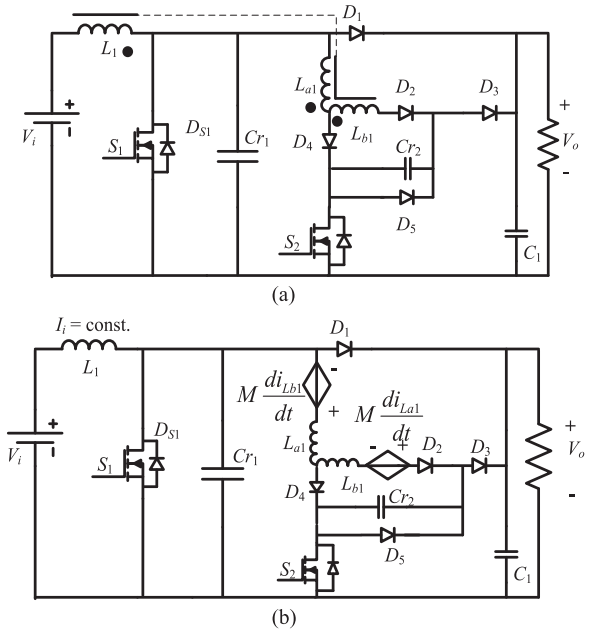

Fig. 1. Proposed soft-switching boost converter topology. (a) Boost converter. (b) Equivalent circuit.

where v_{L1}, v_{La1}, and v_{Lb1} are the voltages of the coupled inductors; L_1, L_{a1}, and L_{b1} are the inductances of the coupled inductors; M_{a1}, M_{b1}, and M are the mutual inductances of L_1 and L_{a1}, L_1 and L_{b1}, and L_{a1} L_{b1} respectively; i_{L1}, i_{La1}, and $i_{\mathrm{Lb}1}$ are the currents of L_1, L_{a1}, and L_{b1}.

In order to better understand the operating principles of the converter and to simplify the analysis, the output voltage V_{o} and the main inductor current I_{i} are assumed to be constant, due to the large capacitance and inductance involved. Then, the converter equivalent circuit can be modified as shown in Fig. 1(b) for mode analysis with respect to $di_{L1}/dt \approx 0$.

The boost converter's key waveforms are shown in Fig. 2, and it has been analyzed for one PWM period in $(8 + 1)$ operation modes below, where the existence condition of mode X is dependent on circuit parameters. Each operation stage of the topology is given in Fig. 3.

1) Mode 1 [$t_0 \le t < t_1$, Fig. 3(a)]: This mode is the main switching off-stage of the conventional boost converter. In this interval, S_1 and S_2 are in the off-state. The dc power supply charges the main inductor through D_1.

2) Mode 2 [$t_1 \le t < t_2$, Fig. 3(b)]: The initial conditions at t_1 are $v_{Cr1} = V_o$, $v_{Cr2} = 0$, $i_{s1} = 0$, $i_{s2} = 0$, $i_{D1} = I_i$ and $i_{La1} = i_{Lb1} = 0$, and the active signal is applied to the switch S_2 and a resonance starts between L_{a1}, L_{b1} and C_{r2}. For this resonance S_2 starts with ZCS. Meanwhile, the main diode current i_{D1} falls, and the capacitor C_{r2} charges. At the end of this mode, the current in the main diode decreases to zero, so ZCS off of the main diode realizes and the voltage of the capacitor C_{r2} rises. The equations obtained for this mode are given as follows:

$$v_{Cr2} = \frac{M}{L_{a1}} V_o - \frac{M}{L_{a1}} V_o \cos \omega_1 (t - t_1) \tag{2}$$

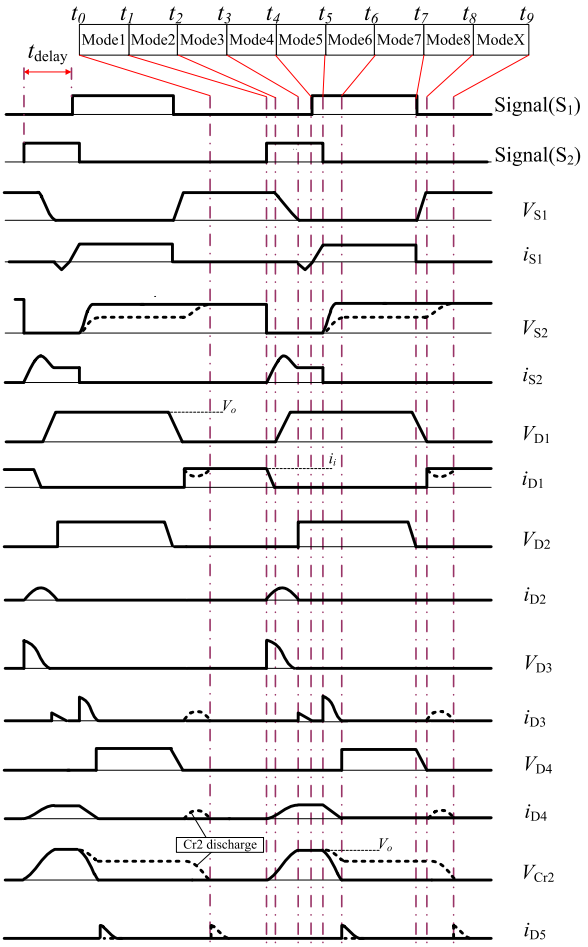

Fig. 2. Key waveforms of operation modes.

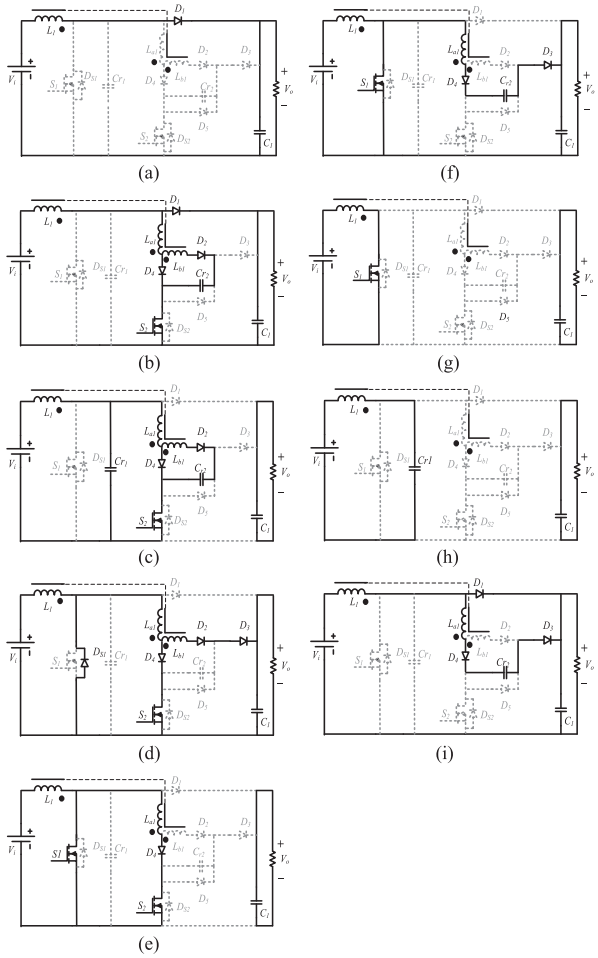

Fig. 3. Topology of operations stages. (a) Mode 1 ($t_0 \le t < t_1$). (b) Mode 2 ($t_1 \le t < t_2$). (c) Mode 3 ($t_2 \le t < t_3$). (d) Mode 4 ($t_3 \le t < t_4$). (e) Mode 5 ($t_4 \le t < t_5$). (f) Mode 6 ($t_5 \le t < t_6$). (g) Mode 7 ($t_6 \le t < t_7$). (h) Mode 8 ($t_7 \le t < t_8$). (i) Mode X ($t_8 \le t < t_9$, exists if voltage of C_{r2} is not zero).

$$i_{Lb1} = \frac{M}{\omega_1(L_{a1}L_{b1} - M^2)} V_o \sin\omega_1(t - t_1) \tag{3}$$

$$i_{La1} = \frac{V_o}{L_{a1}}(t - t_1) + \frac{M^2}{(L_{a1}L_{b1} - M^2)L_{a1}\omega_1} \times V_o \sin\omega_1(t - t_1), \tag{4}$$

where M is the mutual inductance of the L_{a1} and L_{b1}, and $\omega_1 = \sqrt{\frac{L_{a1}}{C_{r2}(L_{a1}L_{b1} - M^2)}}$.

3) Mode 3 [$t_2 \le t < t_3$, Fig. 3(c)]: In mode 3, when diode D_1 turns off, C_{r1}, C_{r2}, L_{1a}, and L_{1b} resonate, so energy stored in the capacitor C_{r1} is transferred to L_{a1}, L_{b1} and C_{r2}. C_{r2} voltage is charged to V_o at the end of this mode. The antiparallel diode of the main switch S_1 will be active when voltage cross C_{r1} falls to zero, and mode 3 finishes.

To simplify the complexity of the calculation, the initial conditions are considered as $v_{Cr1} \approx V_o$, $v_{Cr2} \approx 0$ and $i_{La1} = i_{Lb1} \approx 0$, due to the superfast recovery diode D_1 and the short duration between t_2 and t_3. Then for this resonance, the following equations exist:

$$i_{Lb1} = -A_1 C_{r1} V_o \omega_{21} \sin\omega_{21} t + A_1 C_{r1} V_o \omega_{22} \sin\omega_{22} t + A_1 I_i \cos\omega_{21} t - A_1 I_i \cos\omega_{22} t \tag{5}$$

$$v_{Cr2} = A_2 C_{r1} V_o \cos\omega_{21} t - A_2 C_{r1} V_o \cos\omega_{22} t + \frac{A_2 I_i \sin\omega_{21} t}{\omega_{21}} - \frac{A_2 I_i \sin\omega_{22} t}{\omega_{22}} \tag{6}$$

where: un. eqn shown at the bottom of the next page.

$$A_1 = \frac{C_{r2} M}{\sqrt{(C_{r1}L_{a1} - C_{r2}L_{b1})^2 + 4C_{r1}C_{r2}M^2}},$$

$$A_2 = \frac{M}{\sqrt{(C_{r1}L_{a1} - C_{r2}L_{b1})^2 + 4C_{r1}C_{r2}M^2}}.$$

4) Mode 4 [$t_3 \le t < t_4$, Fig. 3(d)]: In this mode, D_{S1} is at the turn-on stage. After the voltage of C_{r2} reaches the output voltage at the end of mode 3, D_3 is active with ZVS and current of L_{b1} continues, so energy is transferred to the load through diode D_3 from the coupled inductor. The current stress of S_2 is reduced obviously. Because the current of L_{b1} decreases slowly to zero, diode D_3 turns off at ZCS. At $t = t_3$, the initial conditions are $v_{Cr2} = V_o$, $i_{s1} = 0$, $i_{La1} = I_{La1_3}$ and $i_{Lb1} = I_{Lb1_3}$.

The following equations are valid in this mode:

$$i_{La1} = I_{La1\_3} - \frac{M}{L_{a1}L_{b1} - M^2} V_o(t - t_3) \tag{7}$$

$$i_{Lb1} = I_{Lb1\_3} - \frac{M}{L_{a1}L_{b1} - M^2} V_o(t - t_3). \tag{8}$$

5) Mode 5 [$t_4 \le t < t_5$, Fig. 3(e)]: In the interval when the antiparallel diode D_{S1} is active, the turn-on signal for the main switch S_1 is applied at ZVZCT, and this mode starts. At the beginning of this mode, current in L_{b1} and D_3 has been reduced to zero at ZCS, meanwhile the $i_{La1} - I_i$ freewheeling current in D_{S1} continues to fall. There exist the following equations:

$$i_{La1} = i_{S2} \tag{9}$$

$$i_{DS1} = i_{La1} - I_i. \tag{10}$$

The interval before which $i_{La1} - I_i$ drops to zero provides the turn-on control margin for the main switch. The signal will be applied to provide ZVZCT turn-on of S_1 when its antiparallel diode is active.

6) Mode 6 [$t_5 \le t < t_6$, Fig. 3(f)]: At the beginning of this mode, the control signal of S_2 is removed. L_{a1} and C_{r2} start to resonate. Capacitor C_{r2} discharges from V_o. S_2 turns off with ZVS because the voltage of S_2 (v_{S2}) in this mode is equal to $v_{Cr1} + v_{C1}$ with the parasitic capacitor. The voltage cross capacitor C_{r2} resonates to zero, the parallel diode D_5 will turn on with ZVS and help release the rest energy of L_{a1}. At $t = t_5$, $v_{Cr1} = 0$, $v_{Cr2} = V_o$, $i_{S2} = 0$, $i_{D1} = 0$, and $i_{La1} = I_{La1_5}$. In this situation, the following equations are derived:

$$v_{Cr2} = \frac{I_{La1\_5}}{C_{r2}\omega_5} \sin\omega_5(t - t_5) - V_o \tag{11}$$

$$i_{La1} = I_{La1\_5} \cos\omega_5(t - t_5) \tag{12}$$

$$v_{s2} = v_{Cr2} + v_{C1} = \frac{I_{La1\_5}}{C_{r2}\omega_5} \sin\omega_5(t - t_5) \tag{13}$$

where $\omega_5 = \frac{1}{\sqrt{C_{r2}(L_{a1} + M)}}$. Equation (13) shows that switch S_2 realizes ZVS turn-off successfully.

7) Mode 7 [$t_6 \le t < t_7$, Fig. 3(g)]: This mode is a conventional PWM mode. The power supply and the inductor L_1 organize an isolated circuit, and the output capacitor C_1 supplies for the load power.

8) Mode 8 [$t_7 \le t < t_8$, Fig. 3(h)]: This mode starts by removing the control signal of S_1, and the main switch is turned off with ZVS due to the parallel capacitor C_{r1}. The diode D_1 turns on with ZVT as well. The C_{r1} voltage can be expressed as follows:

$$v_{Cr1} = \frac{I_i}{C_{r1}}(t - t_7). \tag{14}$$

Once the v_{Cr1} reaches V_o, this mode ends. The duration of this mode is expressed as:

$$t_{7-8} = \frac{V_o C_{r1}}{I_i}. \tag{15}$$

9) Mode X [$t_8 \le t < t_9$, Fig. 3(i)]: The uncertain mode X will exist if the voltage cross C_{r2} does not resonate to zero in mode 6. After charging C_{r1} completes, C_{r2} will discharge to zero voltage, and current across L_{a1} will continue to go through diode D_5. Obviously, D_5 is also under SS in this mode. At $t = t_8$, $v_{Cr2} = V_{Cr2_8}$. The current i_{La1}, and the voltage v_{Cr2} can be calculated as:

$$i_{La1} = \sqrt{\frac{C_{r2}}{L_{a1}}} V_{Cr2\_8} \sin\omega_8(t - t_8) \tag{16}$$

$$v_{Cr2} = V_{Cr2\_8} \cos\omega_8(t - t_8) \tag{17}$$

where $\omega_8 = \frac{1}{\sqrt{C_{r2}L_{a1}}}$.

Mode X existence condition below should be satisfied.

$$\frac{1}{2}L_{a1}{I_{a1\_5}}^2 \le \frac{1}{2}C_{r2}{V_o}^2 \tag{18}$$

where I_{a1_5} is the current across L_{a1} at the instant t_5. At $t = t_9$, one PWM period ends and the next one starts.

III. Parameter Analysis

A. Conditions of Turn-On With ZVZCT and Turn-Off With ZVS for the Main Switch

The ZVS turn-off condition of S_1 is always satisfied due to existence of C_{r1}. However, before the signal of the auxiliary switch is removed, C_{r1} must be discharged completely. The driver signal of the main switch will be applied when the body diode is in the on-state, such that the main switch will be turned on with ZVZCT. Furthermore, the discharging time interval for C_{r1} should not be longer than $t_3 - t_2$. Thus, the following conditions must be achieved for the ZVZCT turn-on of the main switch S_1:

$$I_{La1\_3} - I_i \ge 0 \tag{19}$$

$$C_{r1} \le \frac{I_i}{V_o}(t_3 - t_2). \tag{20}$$

As shown in Fig. 2, the active signal of the main switch delays the auxiliary switch. The delay time complies with the following

$$\omega_{21} = \frac{\sqrt{-\sqrt{(C_{r1}L_{a1} - C_{r2}L_{b1})^2 + 4C_{r1}C_{r2}M^2} + C_{r1}L_{a1} + C_{r2}L_{b1}}}{\sqrt{2C_{r1}C_{r2}(L_{a1}L_{b1} - M^2)}}$$

$$\omega_{22} = \frac{\sqrt{\sqrt{(C_{r1}L_{a1} - C_{r2}L_{b1})^2 + 4C_{r1}C_{r2}M^2} + C_{r1}L_{a1} + C_{r2}L_{b1}}}{\sqrt{2C_{r1}C_{r2}(L_{a1}L_{b1} - M^2)}}$$

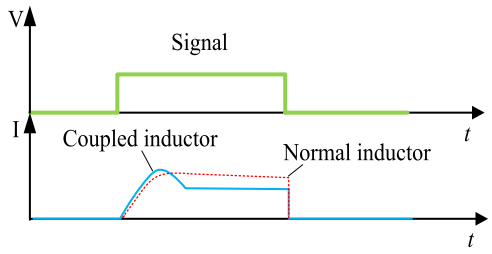

Fig. 4. Current and voltage waveforms using different inductors.

condition:

$$(t_3 - t_0) < t_{\text{delay}} < t|_{iDs1=0} \tag{21}$$

where $t|_{iDs1=0}$ is the moment at which i_{Ds1} falls to zero, and t_3 is the moment when voltage of C_{r1} resonate to zero.

B. Conditions of Turn-On With ZCS and Turn-Off With ZVS for the Auxiliary Switch

The rising rate of the current is limited due to the coupled inductors. Therefore, the turn-on of the auxiliary switch is achieved with ZCS. The resonance between C_{r2} and L_{a1} occurs when the auxiliary switch is in the off-state. Whether the voltage of C_{r2} can resonate to V_o is critical to the ZVS realization of S_2. Because it determines the initial voltage ($v_{S2} = v_{Cr1} + v_{C1}$) of the resonance which ought to be zero at the beginning of mode 6.

The least conditions also should be achieved to turn on the auxiliary switch S_2 under ZCS according to (2), (6), and (13):

$$M \geq L_{a1}. \tag{22}$$

Due to the fact that the average charging current of C_{r2} should be slightly lower than the input current I_i, the following relationship is derived:

$$C_{r2} \leq \frac{I_i}{V_o}(t_3 - t_1). \tag{23}$$

C. Coupled Inductor and Capacitor Selection for Soft-Switching Realization

According to the equivalent circuit in Fig. 1(b), one function of the coupled inductor is that $M \cdot di_{La1}/dt$ could be regarded as a controlled voltage source to charge the capacitor C_{r2}, which plays the most important role for ZVS turn-off of the auxiliary switch S_2. Consequently, the stored energy in C_{r2} can be transferred to the converter output in mode 6.

In addition, part of energy in L_{a1} is transferred to the output directly in mode 4 because of the existence of $M \cdot di_{L1a}/dt$. When i_{L1b} increases, the coupling effect due to $M \cdot di_{L1b}/dt$ helps the main switch achieve the ZVZCT condition more easily at a wide load range, according to the first condition of (19). When i_{L1b} decreases, $M \cdot di_{L1b}/dt$ becomes a negative value, effectively suppressing the reverse current of the main switch. Meanwhile, the auxiliary switch current will be less than that with the same-size independent inductance, resulting in loss reduction (as shown in Fig. 4). With respect to the mutual inductance *M* and the polarity of $M \cdot di_{L1a}/dt$ and $M \cdot di_{L1b}/dt$ shown in Fig. 1(b), the dotted terminals of the coupled inductor should be connected.

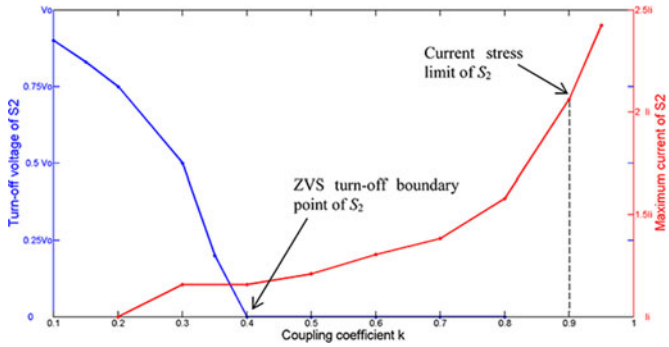

Fig. 5. Influence of coupling coefficient on the maximum current and turn-off voltage of S_2.

Considering the effect of the controlled voltage source $M \cdot di_{L1b}/dt$, selection of a proper M may control reverse current in D_{s1} and the current stress of S_2. So a little smaller mutual inductance selection with regard of $M \geq L_{1a}$ [according to (22)] will reduce the auxiliary switch current stress and improve the efficiency accordingly.

Coupled inductors could be wired using different material with high frequency, e.g., ring-type ferrite core MnFe204, ZnFe204, etc. In practice, the coupling coefficient using the ring core is not easy to reach over 0.95, and the coupling coefficient will decrease when enlarging the distance between L_{a1} and L_{b1}. To carefully tune the distance between two windings could help obtain the relatively precise coupling coefficient.

As shown in Fig. 5, if the coupling coefficient is close to 1 or larger than 0.9, the peak current of S_2 is unacceptably high. If the coupling coefficient is smaller than 0.4, there will not be ZVS in S_2. So the best choice is to both consider the maximum current on S_2 and satisfy the complete ZVS for S_2. Commonly, the mode 4 existing means i_{Lb1} is larger than zero and the C_{r2} has already been charged to the V_o. By the critical condition, the minimum value of coupling coefficient could be estimated. Consequently, L_{a1} and L_{b1} can be estimated using the following expressions:

$$\begin{cases} i_{La1} - I_i = I_{La1\_3} - \dfrac{M}{L_{a1}L_{b1} - M^2}V_o(t - t_3) - I_i \geq 0 \\ k \in [0.4,\ 0.9] \\ k = \dfrac{M}{\sqrt{L_{a1}L_{b1}}} \\ M \geq L_{a1} \end{cases}. \tag{24}$$

C_{r1} includes the parallel capacitor and the parasitic capacitors of S_1 and D_1. According to (13), the parasitic capacitor of S_2 must be considered as being in parallel with C_{r2} and C_1. Equations (19)–(20) and (23) provide conditions of ZVZCT turn-on for the main switch and ZVS turn-off for the auxiliary switch, respectively.

C_{r2} affects the SS range of the switches. Due to (13) and (19), $(v_{Cr2} - V_o)/V_o$ and $i_{La1} - I_i$ could be considered as the SS boundary conditions for the main and auxiliary

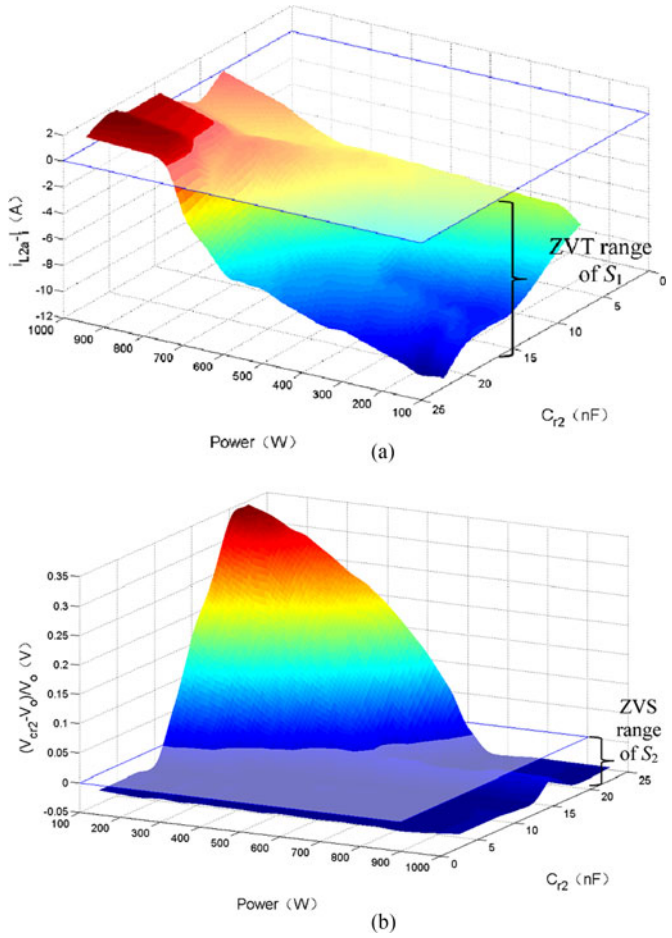

Fig. 6. SS range of main and auxiliary switches with different parameters. (a) ZVZCT range of the main switch S_1. (b) ZVS range of the auxiliary switch S_2.

switches, respectively. Fig. 6 shows the relationship among SS, capacitor C_{r2}, and load with the input voltage 100 V. It is observed Cr_2 could not too large, which not only affects the switch ZVT boundary, but also affects the main switch recovery current. Obviously, a proper selection for C_{r2} will guarantee SS conditions in a very wide load range.

IV. Experimental Results

To verify the aforementioned analysis, a prototype of the proposed converter has been built. The specifications of the experimental conditions and circuit parameters of the proposed converter are presented in Table I.

Fig. 7 shows the photograph of the proposed converter prototype. This boost converter is composed of a main inductor (L_1) coupled with the resonance inductors, a main transistor with body diode, and a main diode. The output capacitance C_1 is chosen the value of 560 μF. The switching frequency is set to 100 kHz, and the PWM duty cycle is 0.48 generated by the control board TMS320F28335. The input and output voltages are 100 and 200 V, respectively. The maximum power is 1 kW.

The maximum power level is actually the hardest condition to realize SS for the converter seen from the Fig. 6(a). Since the maximum and light load tests are both done, the load range is

TABLE I
Experimental Conditions and Circuit Parameters

Symbols	Descriptions	Specifications
S_1,	Main switch	IPW60R041C6
S_2	Auxiliary switch	IXFK55N50
$D_1 - D_5$	Diodes	RHRP30120x5
C_{r1}, C_{r2}	Resonant capacitors	4.5 nF, 5 nF
L_1, L_{a1}, L_{b1}	Coupled inductors	0.25 mH, 7 µH, 16 µH
k_{ab}, k_{a1}, k_{b1}	Coupling coefficients	0.83, 0.41, 0.32
S_1,	Main switch	IPW60R041C6
S_2	Auxiliary switch	IXFK55N50

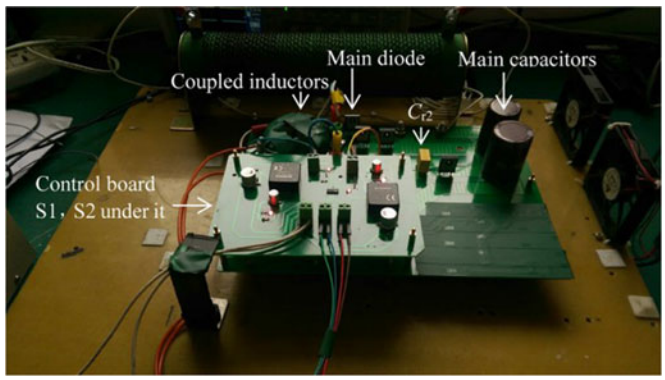

Fig. 7. Proposed converter.

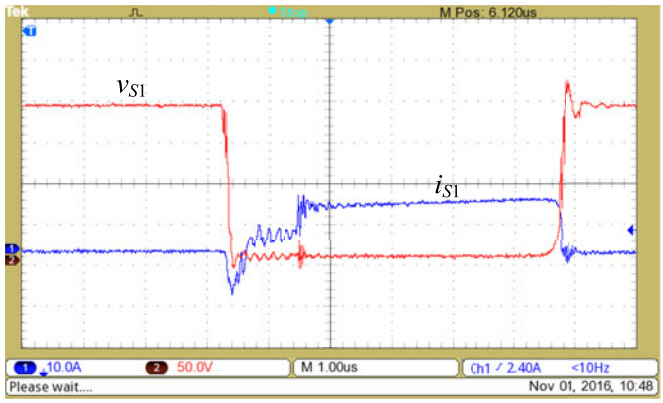

Fig. 8. Voltage and current of S_1.

fully covered. Typical waveforms of current and voltage can be found in Figs. 8–14. The main switch voltage and current waveforms for the turn-on and turn-off processes are shown in Fig. 8. In Fig. 8, v_{S1} reduces to zero before the gate triggering signal of S_1 is applied, and then the current reverses and increases from zero, so the ZVZCT turn-on of S_1 is achieved. In Fig. 8, when the turn-off signal is applied, i_{S1} decreases quickly to zero, and then, v_{S1} increases. Therefore, ZVS is also achieved in the turn-off process. Fig. 9 shows the turn-on and turn-off processes of S_2. Current increases smoothly when the active signal of S_2 is applied, so S_2 turns on under ZCS. It also can be seen from this figure that when the switching signal is removed, i_{S2} decreases quickly to zero, after that, v_{S2} increases to V_o, and ZVS is also valid. In Fig. 14, it could be seen that when the mode X existence conditions is satisfied, capacitor C_{r2} discharges again in

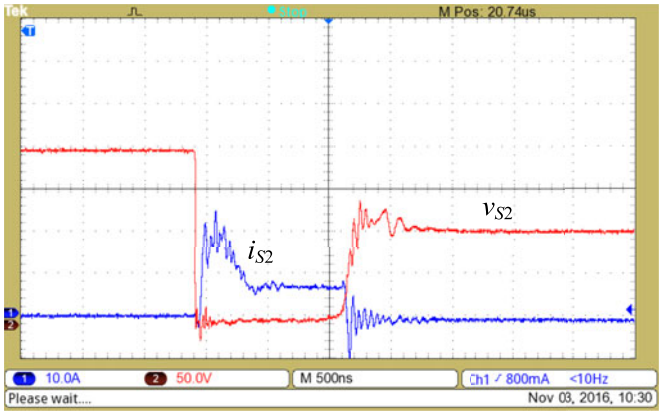

Fig. 9. Voltage and current of S_2.

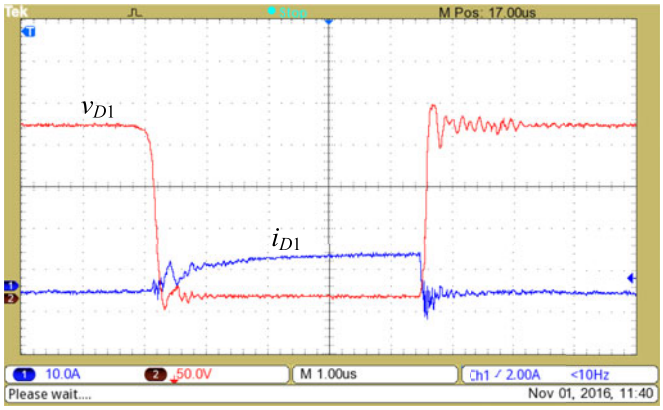

Fig. 10. Voltage and current of D_1.

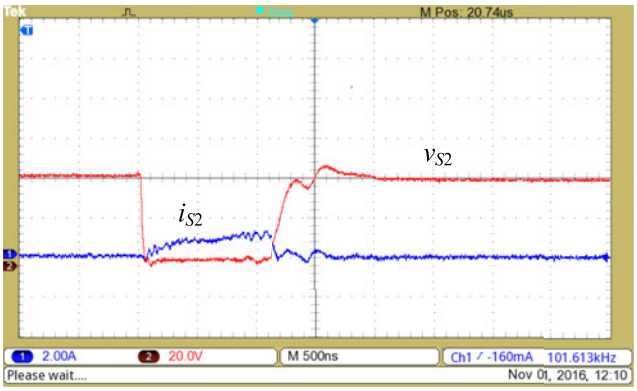

Fig. 11. Voltage and current of S_2 without mode X.

mode X, and the auxiliary switch voltage rises to V_o after the main switch turns off. Fig. 11 shows that when mode X does not exist, the auxiliary switch voltage rises to the output voltage immediately after the auxiliary switch is off. As Fig. 10 shows, the main diode operates in the soft-switching state. The rest diodes are also at the soft-switching state. Therefore, the efficiency of the converter is improved additionally. It can be seen in Figs. 13 and 14 that the same SS situation of the switches exists for the light load (one-fifth of the maximum load). Fig. 12 shows that the use of the coupled inductor can help transfer energy to the

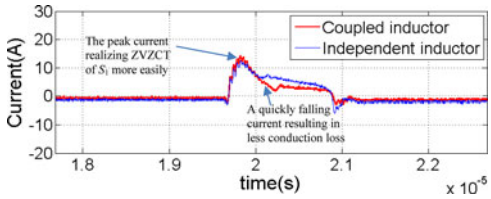

Fig. 12. Auxiliary switch current with different inductors.

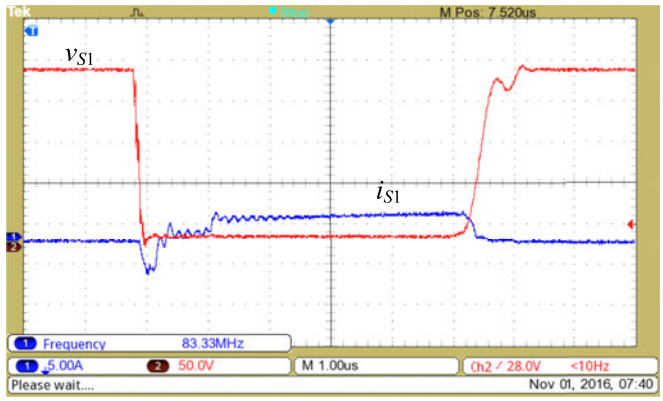

Fig. 13. Voltage and current of S_1 and the output at a light load (one-fifth of full load).

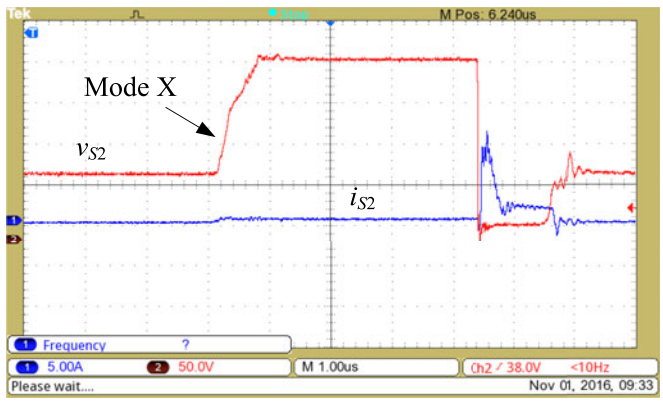

Fig. 14. Voltage and current of S_2 and the input at light load (one-fifth of full load).

converter output, so a quick fall and the small average current of S_2 due to the coupling effect reduce circulating cost compared with that using an independent inductor. Furthermore, the peak current providing for $(i_{La1} - I_i \geq 0)$ expands the ZVZCT condition for S_1 of the load range and overcomes the input current affection due to the coupling effect.

The efficiency of the proposed converter is measured by a power analyzer (WT-1800). The efficiency curve of the proposed converter is shown in Fig. 15, which demonstrates that high efficiency can be obtained in a wide load range. At the maximum load, the peak efficiency reaches 97.4%. In the meantime, soft-switching could be implemented at light load, and efficiency of 92% at only one-fifth maximum load is reached. The efficiency of the proposed converter is higher than that of the soft-switching converter using an independent inductor, which is consistent with the fact that efficiency is improved additionally since the

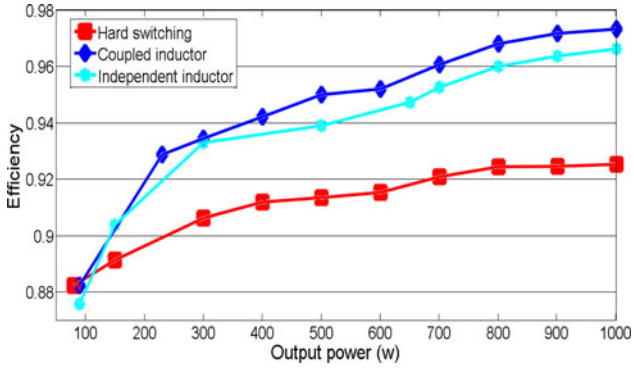

Fig. 15. Efficiency comparison.

energy in the resonance circuit can be transferred to the converter output and reduces average conduction current of the auxiliary switch thanks to the coupling effect.

V. Conclusion

In this paper, a novel boost ZVZCT soft-switching converter topology is proposed. This converter provides the main switch ZVZCT at the turn-on process and ZVS at the turn-off, also the auxiliary switch turns on at the ZCS and turns off at the ZVS. All the diodes could operate under soft-switching conditions. The main switch is not subjected to additional voltage and current stresses. Meanwhile, there is no additional voltage stress on the auxiliary switch, and its current stress is at an acceptable level. The prototype of the proposed converter has been built, and the experimental results verify the soft-switching realization. The efficiencies are better in a wide range than those in the conventional or independent-inductor-based converter, which is in accord with the theoretical analysis derived in this paper.

Appendix

The derivation process for some solutions in Section II regarding the circuit state equations is provided in Appendix. In mode 2, the differential equations according to the Kirchhoff voltage law (KVL) and Kirchhoff current law (KCL) are listed as follows:

$$V_0 = \left[L_{a1} - 2M + \frac{(L_{a1}-M)(L_{b1}-M)}{M} + L_{b1}\right] \times \frac{di_{Lb1}}{dt} + \left(\frac{L_{a1}-M}{M}+1\right) u_{cr2} \tag{A1}$$

$$C_{r2}\frac{du_{cr2}}{dt} = i_{Lb1}. \tag{A2}$$

The initial conditions at $t = t_1$ are $v_{Cr1} = V_o$, $v_{Cr2} = 0$, $i_{s1} = 0$, $i_{s2} = 0$, $i_{D1} = I_i$ and $i_{La1} = i_{Lb1} = 0$.

In mode 3, we list the differential equation related to KVL and KCL as follows:

$$C_{r1}\frac{dV_{Cr1}}{dt} = I_i - i_{La1} \tag{A3}$$

$$C_{r2}\frac{dV_{Cr2}}{dt} = i_{Lb1} \tag{A4}$$

$$\frac{L_{a1}L_{b1}-M^2}{M}\frac{di_{Lb1}}{dt} + \frac{L_{a1}}{M}V_{Cr2} = V_{Cr1} \tag{A5}$$

$$M\frac{di_{Lb1}}{dt} = L_{b1}\frac{di_{Lb1}}{dt} + V_{Cr2}. \tag{A6}$$

The initial conditions for this equation set are considered as $v_{Cr1} \approx V_o$, $v_{Cr2} \approx 0$ and $i_{La1} = i_{Lb1} \approx 0$.

In mode 6, the following differential equations are obtained:

$$L_{1a}\frac{di_{L1a}}{dt} + u_{Cr2} + V_o = 0 \tag{A7}$$

$$C_{r2}\frac{du_{Cr2}}{dt} = i_{La1}. \tag{A8}$$

At $t = t_5$, we have the initial conditions as $v_{Cr1} = 0$, $i_{S2} = 0$, $i_{D1} = 0$, $i_{_{L1a}} = I_{L1a\_5}$, and $u_{Cr2} = -V_o$

In mode X, at $t = t_8$, there exist $v_{Cr2} = V_{Cr2_8}$ and $i_{La1} = 0$, and the state equations are depicted as follows:

$$L_{a1}\frac{di_{La1}}{dt} = v_{Cr2} \tag{A9}$$

$$C_{r2}\frac{dv_{Cr2}}{dt} = i_{La1}. \tag{A10}$$

References

[1] P. Thounthong, "Control of a three-level boost converter based on a differentia flatness approach for fuel cell vehicle applications," *IEEE Trans. Veh. Technol.*, vol. 61, no. 3, pp. 1467–1472, Mar. 2012.

[2] F. Musavi, W. Eberle, and W. G. Dunford, "A high-performance single phase bridgeless interleaved PFC converter for plug-in hybrid electric vehicle battery chargers," *IEEE. Trans. Ind. Appl.*, vol. 47, no. 4, pp. 1833–1843, Jul./Aug. 2011.

[3] Y. K. Lo, C. Y. Lin, H. J. Chiu, S. J. Cheng, and J. Y. Lin, "Analysis and design of a push-pull quasi-resonant boost power factor corrector," *IEEE Trans. Power Electron.*, vol. 28, no. 1, pp. 347–356, Jan. 2013.

[4] M. Pahlevaninezhad, P. Das, J. Drobnik, P. K. Jain, and A. Bakhshai, "A ZVS interleaved boost AC/DC converter used in plug-in electric vehicles," *IEEE Trans. Power Electron.*, vol. 27, no. 8, pp. 3513–3529, Aug. 2012.

[5] S. H. Park, G. R. Cha, Y. C. Jung, and C. Y. Won, "Design and application for PV generation system using a soft-switching boost converter with SARC," *IEEE Trans. Ind. Electron.*, vol. 57, no. 2, pp. 515–522, Feb. 2010.

[6] D. Y. Jung, Y. H. Ji, S. H. Park, Y. C. Jung, and C. Y. Won, "Interleaved soft-switching boost converter for photovoltaic power-generation system," *IEEE Trans. Power Electron.*, vol. 26, no. 4, pp. 1137–1145, Apr. 2011.

[7] N. R. Newlin, A. Jenifer, G. Rohini, and V. Jamuna, "Digital simulation of single and interleaved soft switching boost converter for PV," in *Proc. Int. Conf. Comput., Electron. Electr. Technol.*, 2012, pp. 307–313.

[8] S. H. Park, S. R. Park, J. S. Yu, Y. C. Jung, and C. Y. Won, "Analysis and design of a soft-switching boost converter with an hi-bridge auxiliary resonant circuit," *IEEE Trans. Power Electron.*, vol. 25, no. 8, pp. 2142–2149, Aug. 2010.

[9] N. Altintas, A. Faruk Bakan, and I. Aksoy, "A novel ZVT-ZCT-PWM boost converter," *IEEE Trans. Power Electron.*, vol. 29, no. 1, pp. 256–265, Jan. 2014.

[10] D. W. Han, H. J. Lee, and S. C. Shin, "A new soft switching ZVT boost converter using auxiliary resonant circuit," in *Proc. IEEE Veh. Power Propulsion Conf.*, 2012, pp. 1250–1255.

[11] Y.-W. Kim, J.-H. Kim, K.-Y. Choi, and B.-S. Suh, "A novel soft switched auxiliary resonant circuit of a PFC ZVT-PWM boost converter for an integrated multichip power module fabrication," *IEEE Trans. Ind. Appl.*, vol. 49, no. 6, pp. 2802–2809, Nov./Dec. 2013.

[12] A. F. Bakan, H. Bodur, and I. Aksoy, "A novel ZVT-ZCT PWM DC-DC converter," in *Proc. 11th Eur. Conf. Power Electron. Appl.*, 2005, Art. ID. 1665652.

[13] C. M. Wang, C. H. Lin, H. C. Kuo, and C. I. Lin, "Zero-current transition interleaved boost DC/DC converter," in *Proc. IEEE Conf. Ind. Electron. Appl.*, 2014, pp. 278–281.

[14] P. Das and G. Moschopoulos, "A comparative study of zero-current transition PWM converters," *IEEE Trans. Ind. Electron.*, vol. 54, no. 3, pp. 1319–1328, Jun. 2007.
[15] B. Akın, "An improved ZVT–ZCT PWM DC-DC boost converter with increased efficiency," *IEEE Trans. Power Electron.*, vol. 29, no. 4, pp. 1919–1926, Apr. 2014.
[16] B. Akın and H. Bodur, "A new single-phase soft-switching power factor correction converter," *IEEE Trans. Power Electron.*, vol. 26, no. 2, pp. 436–443, Feb. 2011.
[17] T. Mishima, Y. Takeuchi, and M. Nakaoka, "Analysis, design, and performance evaluations of an edge-resonant switched capacitor cell-assisted soft-switching PWM boost DC-DC Converter and its interleaved topology," *IEEE Trans. Power Electron.*, vol. 28, no. 7, pp. 3363–3378, Jul. 2013.
[18] W. Li and X. He, "High step-up soft switching interleaved boost converters with cross-winding-coupled inductors and reduced auxiliary switch number," *IET Power Electron*., vol. 2, no. 2, pp. 125–133, Mar. 2009.
[19] Y. C. Hsieh, T. C. Hsueh, and H. C. Yen, "An interleaved boost converter with zero-voltage transition," *IEEE Trans. Power Electron.*, vol. 24, no. 4, pp. 973–978, Apr. 2009.
[20] D. Y. Jung, Y. H. Ji, S. H. Park, Y. C. Jung, and C. Y. Won, "Interleaved soft-switching boost converter for photovoltaic power-generation system," *IEEE Trans. Power Electron.*, vol. 26, no. 4, pp. 1137–1145, Apr. 2011.
[21] Y. T. Chen, S. M. Shiu, and R. H. Liang, "Analysis and design of a zero-voltage-switching and zero-current-switching interleaved boost converter," *IEEE Trans. Power Electron.*, vol. 27, no. 1, pp. 161–173, Jan. 2012.
[22] J. Zhang, J. S. Lai, R. Kim, and W. Yu, "High-power density design of a soft-switching high-power bidirectional DC-DC converter," *IEEE Trans. Power Electron.*, vol. 22, no. 4, pp. 1145–1153, Jul. 2007.
[23] W. Yu, H. Qian, and J. S. Lai, "Design of high-efficiency bidirectional DC-DC converter and high-precision efficiency measurement," *IEEE Trans. Power Electron.*, vol. 25, no. 3, pp. 650–658, Mar. 2010.
[24] Y. Gu and D. Zhang, "Interleaved boost converter with ripple cancellation network," *IEEE Trans. Power Electron.*, vol. 28, no. 8, pp. 3860–3869, Aug. 2013.
[25] K. J Lee, B. G. Park, R. Kim, and D. S. Hyun, "Nonisolated ZVT two inductor boost converter with a single resonant inductor for high step-up applications," *IEEE Trans. Power Electron.*, vol. 27, no. 4, pp. 1966–1973, Apr. 2012.
[26] A. Mirzaei, A. Jusoh, Z. Salam, E. Adib, and H. Farzanehfard, "A novel soft switching bidirectional coupled inductor buck-boost converter for battery discharging-charging," in *Proc. IEEE Appl. Power Electron. Colloq.*, 2011, pp. 195–199.
[27] S. Urgun, "Zero-voltage transition-zero-current transition pulse width modulation DC-DC buck converter with zero-voltage switching-zero-current switching auxiliary circuit," *IET Power Electron.*, vol. 5, no. 5, pp. 627–634, May 2012.

Xi Zhang (M'08–SM'13) received the B.Sc. degree in applied mathematics and the B.E. degree in information and control engineering from Shanghai Jiao Tong University (SJTU), Shanghai, China in 2002. He received the M.E. and Ph.D. degrees in power electronics and electric power drive from SJTU, in 2004 and 2007, respectively.

From September 2007 to July 2009, he held a Postdoctoral position with the Department of Electrical and Computer Engineering, University of Michigan-Dearborn, Dearborn, MI, USA. He is currently an Associate Professor with the Institute of Automotive Engineering and National Engineering Lab for Automotive Electronics and Control Technology, SJTU. His research interests include battery management systems, power electronics devices, and electric motor control systems for alternative-fuel vehicles.

Wei Qian received the B.S. degree in mechanical engineering and automation and the M.S. degree in aircraft design from Nanjing University of Aeronautics & Astronautics, Nanjing, China, in 2005 and 2013, respectively. He is currently working toward the Ph.D. degree at the School of Mechanical Engineering, Shanghai Jiao Tong University, Shanghai, China.

His research interests include soft-switching power converters, power electronics devices, and electric motor control systems.

Zhe Li received the B.E. degree in mechanical engineering and automation from the Department of Mechanical Engineering, Zhengzhou University, Zhengzhou, China, in 2012. He is currently working toward the Ph.D. degree in mechanical engineering at the School of Mechanical Engineering, Shanghai Jiao Tong University, Shanghai, China.

His research interests include the soft-switching power converters and inductive-based wireless power transfer systems.